

PPPL-2416

PPPL-2416


UC20-G

CURRENT RELAXATION TIME SCALES IN TOROIDAL PLASMAS

By

D. R. Mikkelsen

FEBRUARY 1987

PLASMA  
PHYSICS  
LABORATORY 

PRINCETON UNIVERSITY  
PRINCETON, NEW JERSEY

PREPARED FOR THE U.S. DEPARTMENT OF ENERGY,  
UNDER CONTRACT DE-AC02-76-CB0-3073.

# CURRENT RELAXATION TIME SCALES IN TOROIDAL PLASMAS

D. R. Mikkelsen

Plasma Physics Laboratory, Princeton University

Princeton, N.J. 08544

PPPL--2416

DE87 008074

## ABSTRACT

An approximate normal mode analysis of plasma current diffusion in tokamaks is presented. The work is based on numerical solutions of the current diffusion equation in cylindrical geometry. Eigenvalues and eigenfunctions are shown for a broad range of plasma conductivity profile shapes. Three classes of solutions are considered which correspond to three types of tokamak operation. Convenient approximations to the three lowest eigenvalues in each class are presented and simple formulae for the current relaxation time scales are given.

## DISCLAIMER

This report was prepared as an account of work sponsored by an agency of the United States Government. Neither the United States Government nor any agency thereof, nor any of their employees, makes any warranty, express or implied, or assumes any legal liability or responsibility for the accuracy, completeness, or usefulness of any information, apparatus, product, or process disclosed, or represents that its use would not infringe privately owned rights. Reference herein to any specific commercial product, process, or service by trade name, trademark, manufacturer, or otherwise does not necessarily constitute or imply its endorsement, recommendation, or favoring by the United States Government or any agency thereof. The views and opinions of authors expressed herein do not necessarily state or reflect those of the United States Government or any agency thereof.

**MASTER**

DISTRIBUTION OF THIS DOCUMENT IS UNLIMITED

## I. INTRODUCTION

The time scale for current diffusion is often the longest plasma time scale in a tokamak. It therefore plays an important role in large tokamak design and operation. In the TFCX preconceptual design study,<sup>1</sup> for example, the lengths of the lower-hybrid-driven current rampup and ignited burn phases were determined by current diffusion time scales.

An understanding of current relaxation is also required in interpreting the results of noninductive current drive experiments where purely external measurements of the toroidal electric field are used to infer the inductively driven current inside the plasma. Such a procedure is valid only if the inductively driven current has reached its equilibrium value.

The current relaxation time scale is often referred to as the "skin time." The purpose of the present work is to endow that phrase with quantitative meaning in the context of typical tokamak operation. This is done by solving a normal mode problem for each of three types of tokamak operation; the eigenvalues of the normal modes are then related to the current relaxation time scales.

The normal mode problem is defined in Sec. II. A dimensionless eigenvalue equation is derived from the cylindrical current diffusion equation, and three classes of boundary conditions are derived for three types of tokamak operation. Analytic solutions (involving Bessel functions) are presented in Sec. III for the special case of spatially constant plasma conductivity.

The numerical solution of the eigenvalue problem with more realistic conductivity profiles is described in Sec. IV, and the results are presented in Sec. V. Convenient approximations for the current relaxation time scales are presented in Sec. V.D. A brief discussion of the effects of sawteeth is given in Sec. VI.

## II. FORMULATION OF THE DIMENSIONLESS DIFFUSION EQUATION AND BOUNDARY CONDITIONS

The equation for the radial diffusion of the toroidal current density is derived from Maxwell's equations and an Ohm's law. We start with

$$\vec{\nabla} \times \vec{E} = - \frac{\partial \vec{B}}{\partial t} , \quad (1)$$

$$\vec{\nabla} \times B = \mu \vec{j} , \quad (2)$$

where the displacement current has been dropped from the second equation. Tokamak geometry is approximated throughout this work by cylindrical geometry; toroidal mode-coupling, elongation, and triangularity, etc., are ignored. The "toroidal" current density is assumed to be related to the "toroidal" electric field by a simple Ohm's law:

$$j(r,t) = j_d(r) + E(r,t) \sigma(r) , \quad (3)$$

where we restrict attention to cases in which the noninductively driven current,  $j_d$ , and the conductivity,  $\sigma$ , are constant in time.

We have implicitly assumed that the driven current is insensitive to changes in the electric field, a condition met by neutral beam current drive, but frequently not met by lower hybrid current drive. Taking the time derivative of Eq. (2) and eliminating  $j$  and  $B$ , we find that

$$\mu \sigma \frac{\partial E}{\partial t} = \frac{1}{r} \frac{\partial}{\partial r} \left( r \frac{\partial E}{\partial r} \right) . \quad (4)$$

One class of general solutions of Eq. (4) may be expressed as

$$E(r,t) = E_0 + \sum_{n=1}^{\infty} E_n(r) \exp(-t/\tau_n), \quad (5)$$

where  $E_0$  is constant in space and time (the other time-independent solution,  $E = a \ln r$ , is unphysical at the origin). Using the relations

$$x = r/a,$$

$$\tilde{\sigma}(x) = \sigma(r=a)/\sigma_0,$$

where  $\sigma_0 = \sigma(r=0)$ , Eq. (5) becomes

$$E(r,t) = E_0 + \sum_{n=1}^{\infty} E_n F_n(x) \exp(-t/\tau_n), \quad (6)$$

where

$$\frac{d}{dx} \left( x \frac{dF_n}{dx} \right) + k_n^2 \tilde{\sigma} x F_n = 0, \quad (7)$$

and

$$k_n^2 = \mu \sigma_0 a^2 / \tau_n. \quad (8)$$

Note that the differential operator of Eq. (7) is Hermitian, and thus: (i) the eigenvalues are real, (ii) the eigenfunctions are orthogonal, and (iii) the eigenfunctions form a complete set of basis functions, and can be used to represent any solution of Eq. (7). We require  $F_n'(0) = 0$  [this follows from

the finiteness of  $j(0)$ , and the normalization of the eigenfunctions is fixed by requiring that  $F_n(0) = 1$ . The second boundary condition which is required to complete the mathematical statement of the problem depends on the physical situation which is being treated. Three commonly occurring types of tokamak operation are discussed next and suitable boundary conditions are given for each case.

#### A. Free current decay

If the toroidal plasma current changes there will be an induced electric field in the direction of the current of magnitude

$$E(r=a) = -L_{\text{ext}} \dot{I}_p / 2\pi R_0, \quad (9)$$

where  $R_0$  is the major radius of the torus and the external inductance is

$$L_{\text{ext}} = \mu R_0 \left[ \ln(8R_0/a) - 2 \right].$$

A toroidal electric field may also be induced by time-varying currents in the ohmic heating and equilibrium field coils. If the changes in the plasma's poloidal beta and internal inductance can be neglected, then the equilibrium field will change in proportion to changes in the plasma current.<sup>2</sup> The electric field produced by the changing equilibrium field will cancel a portion of the self-induced field given by Eq. (9), thereby reducing the effective external inductance of the torus. Thus, if the current in the ohmic heating coils is constant, the plasma current will resistively decay and, under the above conditions, the electric field at the plasma surface will be

$$E(r=a) = -\dot{I}_{\text{ext}}^* \mu \dot{i}_p / 2\pi, \quad (10)$$

where

$$\dot{I}_{\text{ext}}^* = L_{\text{ext}}^* / \mu R_0, \quad (11)$$

and  $L_{\text{ext}}^*$  is the effective external inductance after correcting for the effects of the equilibrium field described above (typically,  $0.5 \leq \dot{I}_{\text{ext}}^* \leq 1$ ).

The current driven by mode  $A_n$  (generic  $F_n + A_n$  for class A) is

$$A_n^I = 2\pi a^2 \sigma_0 \int_0^1 A_n(x) \tilde{\sigma}(x) x dx = -2\pi a^2 \sigma_0 A_n'(x=1) / A_n^2. \quad (12)$$

Now the boundary condition, Eq. (10), can be expressed

$$A_n(x=1) = \dot{I}_{\text{ext}}^* \mu A_n^I / (2\pi A_n^I) = -\dot{I}_{\text{ext}}^* A_n'(x=1), \quad (13)$$

and  $E_0$  in Eq. (5) must be zero.

### B. Constant surface voltage

We find another set of useful solutions in the case of constant surface voltage, e.g., the electric field at the plasma surface is constant in time. The surface electric field is  $E_0$ , and the boundary condition for the eigenfunctions in this case is  $(F_n + B_n)$

$$B_n(x=1) = 0. \quad (14)$$

The eigenfunctions and eigenvalues here are identical to those of case A in the limit that  $l_{\text{ext}}^* \rightarrow 0$ .

### C. Constant plasma current

It is common practice in tokamak operation to maintain a constant plasma current during part of each discharge. This is accomplished by means of feedback controls on the ohmic heating and equilibrium field coils. During the "current flat-top," the current profile and the surface voltage relax to their equilibrium values. The boundary condition for these eigenfunctions is obtained from the requirement that the integrated current driven by each eigenfunction be zero; following Eq. (12) we have  $(A_n + C_n)$

$$C_n'(x=1) = 0. \quad (15)$$

The equilibrium electric field which drives the constant current is, of course,  $E_0$ .

## III. ANALYTIC SOLUTIONS

If the conductivity is uniform across the plasma, the solutions of Eq. (7) are Bessel functions:  $F_n(x) = J_0(k_n x)$ . The eigenvalues,  $k_n$ , are determined by the boundary conditions discussed below.

### A. Free current decay

From Eq. (13), we have

$$J_0'(A_n k_n) = -l_{\text{ext}}^* a_n^k J_0'(A_n k_n) = l_{\text{ext}}^* a_n^k J_1(A_n k_n).$$



The eigenvalues for various values of  $k_{\text{ext}}^*$  are given in Table I,  $A_n^2$  is given to facilitate the calculation of the  $A_n^*$  from Eqs. (8) and (17).

#### B. Constant surface voltage

From Eq. (14), we have

$$J_0(B_n k_n) = 0 .$$

The  $B_n k_n$  are thus the nth roots of  $J_0(x)$ : 2.405, 5.520, 8.654, etc.

#### C. Constant plasma current

From Eq. (15), we have

$$J_0'(C_n k_n) = 0 = J_1(C_n k_n) .$$

The  $C_n k_n$  are thus the nth roots of  $J_1(x)$ : 3.832, 7.016, 10.174, etc.

### IV. NUMERICAL SOLUTION ALGORITHM

The conductivity profile in a typical tokamak is centrally peaked so the preceding analytic solutions are more useful in checking the numerical work described below than in understanding actual tokamaks.

The results of the next section were generated by the "shooting" methods of solving the two-point boundary value problem posed in Sec. II. Specifically, a trial value for  $k_n^2$  is chosen and Eq. (7) is integrated from  $x=0$  to  $x=1$  where the appropriate function of boundary values -  $G \equiv A_n + k_{\text{ext}}^* A_n'$ , or  $B_n$ , or  $C_n'$  - is evaluated [see Eq. (13-15)]. A modified regula falsi algorithm is used to obtain a new trial value of  $k_n^2$  to be used in

integrating Eq. (7); the procedure is repeated until the absolute value of  $G$  is less than  $10^{-4}$ .

The integration is performed by dividing Eq. (8) into a coupled pair of first order differential equations (for  $F_n$  and  $F'_n$ ), and integrating the pair simultaneously using the Euler predictor-corrector method with a fixed step size of  $\Delta x = 10^{-3}$ . The analytic results for the eigenvalues with constant  $\sigma$  were reproduced to within 0.01% by the numerical algorithm.

## V. NUMERICAL RESULTS

The major parametric dependences of the eigenvalues have been distilled from numerical integrations of Eq. (7) employing a wide variety of conductivity profiles. The results are presented as functions of easily measurable characteristics of the conductivity profile: the average conductivity, the peakedness of the conductivity, and an internal inductance parameter.

In the results presented here, three one-parameter families of functions were used to represent the conductivity profile shapes. The three slowest eigenfunctions for each boundary condition class are shown for one family of conductivity profiles. The three lowest eigenvalues for each boundary condition class and all three conductivity families are compared to simple approximate fits, thereby displaying both the approximation error and the family to family variation of the results.

Three one-parameter functions are used below to generate three families of conductivity profile shapes (see Fig. 1):

$$\tilde{\sigma}_1(x) = [1 - x^2]^\alpha,$$

$$\tilde{\sigma}_{II}(x) = \sigma_2(p=1, x),$$

$$\tilde{\sigma}_{III}(x) = \sigma_2(p=4, x),$$

where

$$\sigma_2(p, x) = 1/[1 + (x/\alpha)^{2p}]^{1+1/p}.$$

Families II and III are frequently referred to as "peaked" and "flat" profile shapes (Ref. [3]). The results for the intermediate "broad" shape ( $p=2$ ) are not presented here, but they are similar to those for  $\tilde{\sigma}_I$ .

Within each family, we may vary the peakedness of the profile (Fig. 1) as measured by

$$q^* \equiv \sigma_0 / \langle \sigma \rangle = [2 \int_0^1 \tilde{\sigma}(x) x dx]^{-1}. \quad (16)$$

In equilibrium  $j(r)/\sigma(r) = E$  is a constant function of radius and, hence,

$$q^* = q(a)/q(0).$$

The edge safety factor,  $q(a)$ , is known from external measurements, and if sawteeth are present, then we may assume  $q(0) \sim 1$ . (See Sec. VI for more discussion of the effects of sawteeth.) Thus, we typically have the estimate

$$q^* \sim q(a)/q(0) \sim q(a).$$

This is not strictly correct (equilibrium is prevented by sawteeth), but it is a reasonable estimate of  $q^*$  in the absence of any direct measurement of the plasma conductivity. The alternative method of measuring  $T_e(r)$  and  $Z_{\text{eff}}(r)$  and assuming a theoretical expression for the conductivity is likely to be more uncertain.

In equilibrium the central conductivity is related to the measurable average conductivity by

$$\sigma_0 = q^* \langle \sigma \rangle = q^* \frac{2}{3} I_p R_0 / (V_s a^2) , \quad (17)$$

where  $I_p$  is the inductively driven plasma current,  $R_0$  is the plasma major radius, and  $V_s$  is the surface voltage.

Another useful measure of the peakedness of the conductivity profile is (Fig. 1)

$$k_i^*/2 = \int_0^1 [B_p^*(x)/B_p^*(x=1)]^2 x dx, \quad (18)$$

where

$$B_p^*(x) = (1/x) \int_0^x \tilde{\sigma}(u) u du.$$

In equilibrium, this reduces to

$$k_i^*/2 = k_i/2 ,$$

which is the usual internal inductance parameter.<sup>2</sup>

We can now relate theoretically important, but rarely measured, characteristics of the conductivity profile to measurable quantities. It must be remembered that these relations can be applied only when there is reason to believe that the conductivity profile itself has not substantially changed between the equilibrium and nonequilibrium phases of a discharge. Fortunately, this is frequently the case a notable exception being lower hybrid current drive experiments.

#### A. Free current decay

The first eigenfunction,  $A_1(x)$ , is shown in Fig. 2 for  $\bar{\sigma} = \bar{\sigma}_I$ .  $\ell_{\text{ext}} = 0.5$ ,  $A_2(x)$  and  $A_3(x)$  are shown only for  $\ell_{\text{ext}}^* = 1$ . As dictated by the boundary condition, Eq. (13), the edge values  $A_n(x=1)$  decrease as  $\ell_{\text{ext}}^*$  is lowered; for  $\ell_{\text{ext}}^* = 0$  the  $A_n(x)$  are identical to the  $B_n(x)$  discussed next. Another prominent feature of the solutions is the existence of  $n-1$  zeros of  $A_n(x)$  inside the plasma.

The eigenvalues can be approximated by

$$A_1^{k_1^2} - \tilde{A}_1^{k_1^2} \approx 2.0 q^* / (\ell_{\text{ext}}^* + \ell_1^*/2),$$

$$A_2^{k_2^2} - \tilde{A}_2^{k_2^2} \approx 15 q^*,$$

$$A_3^{k_3^2} - \tilde{A}_3^{k_3^2} \approx 40 q^*.$$

Note that with a typical  $\ell_{\text{ext}}^* \sim 1$ ,  $A_1^{k_1^2}$  is much lower than all other eigenvalues of types A, B, or C except  $B_1^{k_1^2}$ .

### B. Constant surface voltage

As a consequence of the boundary condition, Eq. (14), the  $n$ th node of  $B_n(x)$  occurs at  $x=1$  (Fig. 3). Both the  $A_n(x)$  and  $B_n(x)$  have approximately constant, nonzero slopes in the outer region of the plasma where  $k_n^2 x \sigma(x) \ll 1$ . As  $q^*$  rises and  $\sigma(x)$  becomes more centrally peaked, the oscillatory region of the eigenfunctions becomes more centrally concentrated.

The eigenvalues can be approximated by

$$B_1^{k_1^2} - \tilde{B}_1^{k_1^2} = 1.8 q^* / (\tilde{a}_1^*/2) ,$$

$$B_2^{k_2^2} - \tilde{B}_2^{k_2^2} = 20 q^* ,$$

$$B_3^{k_3^2} - \tilde{B}_3^{k_3^2} = 50 q^* .$$

### C. Constant plasma current

The boundary condition, Eq. (15), is  $C_n'(x=1) = 0$ ; the region of small  $C_n'(x)$  extends from the boundary to the point where  $k_n^2 x \sigma(x)$  is sufficiently large to generate curvature in  $C_n(x)$  (Fig. 4). As a consequence, the  $n$ th zero of  $C_n(x)$  is located well inside the plasma boundary.

The eigenvalues can be approximated by

$$C_1^{k_1^2} - \tilde{C}_1^{k_1^2} = 12 q^* ,$$

$$C_2^{k_2^2} - \tilde{C}_2^{k_2^2} = 40 q^* ,$$

$$C_3^{k_3^2} - \tilde{C}_3^{k_3^2} = 80 q^* .$$

## D. Time constants

Combining Eqs. (8), (16), and (17), we find that

$$\tau_n = \tau_o q^* / k_n^2, \quad (19)$$

where

$$\begin{aligned} \tau_o &= \mu \langle \sigma \rangle a^2 = 2 \mu I_p R_o / V_s \\ &= 2.51 \text{ sec} \left( \frac{I_p}{\text{mA}} \right) \left( \frac{R_o}{\text{m}} \right) \left( \frac{\text{Volt}}{V_s} \right). \end{aligned} \quad (20)$$

Using the  $k_n^2$  approximations to the true eigenvalues produces the following approximations to the time constants:

Class A: Free current decay

$$A \tilde{\tau}_1 = \tau_o (l_{\text{ext}}^* + l_1^*/2)/2, \quad (21a)$$

$$A \tilde{\tau}_2 = \tau_o / 15, \quad (21b)$$

$$A \tilde{\tau}_3 = \tau_o / 40, \quad (21c)$$

Class B: Constant surface voltage

$$B \tilde{\tau}_2 = \tau_o (l_1^*/2) / 1.8, \quad (22a)$$

$$B \tilde{\tau}_2 = \tau_o / 20, \quad (22b)$$

$$B\bar{\tau}_3 = \tau_o/50 \quad , \quad (22c)$$

Class C: Constant plasma current

$$C\bar{\tau}_1 = \tau_o/12 \quad , \quad (23a)$$

$$C\bar{\tau}_2 = \tau_o/40 \quad , \quad (23b)$$

$$C\bar{\tau}_3 = \tau_o/80 \quad . \quad (23c)$$

These approximate expressions differ from the true expressions by a correction factor  $R_n$ , defined by

$$\tau_n = R_n \bar{\tau}_n \quad . \quad (24)$$

This correction factor is shown for all three families of conductivity profiles in case A (Fig. 5) and cases B and C (Fig. 6). Generally, the approximations  $\bar{\tau}_n$ , are within 20% of the  $\tau_n$ .

## VI. EFFECTS OF SAWTEETH

The current redistribution believed to be associated with "sawtooth" internal disruptions<sup>4</sup> takes place on a time scale much shorter than those discussed above, although it affects only the region near the center of the plasma where  $q \sim 1$ . There are two effects of sawteeth discussed here.

The redistribution of plasma during a sawtooth disruption "flattens" the electron temperature - and, hence, the conductivity - profile. This was found



to be insignificant in the sense that the approximate time scales,  $\bar{\tau}_n$ , well represented the results of numerical solutions using conductivity profiles which had been flattened to radii as large as  $r = a/2$ .

The direct redistribution of current during a sawtooth disruption, however, can greatly speed up the global relaxation time scale if it affects a large fraction of the plasma. To illustrate this, the current relaxation during current "flat-top" after current "ramp-up" was simulated using the BALDUR tokamak transport code,<sup>5</sup> with and without a sawtooth current redistribution model. The tokamak parameters are representative of TFTR:  $B_0 = 4$  T,  $R_0 = 2.5$  m,  $a = 0.85$  m,  $Z_{\text{eff}} = 2.0$ ,  $T_e(r) = 3$  keV  $[1-(r/a)^2]^{4/3}$ , and neoclassical resistivity<sup>6</sup> was used. In each of four simulations, the plasma current was ramped from half its final value to  $I_p = 1.93, 2.10, 2.31,$  and  $2.57$  MA in 1.5 sec and held constant for 2 sec. The final  $q(a)$  were 3.9, 2.75, 2.5, and 2.25, respectively. The simulated surface voltages during the 2 sec flat-top are shown in Fig. 7 for simulations with and without sawteeth (only the two lowest  $q(a)$  simulations are shown, in the other two, the sawtooth model had no discernible effect on the surface voltage). The sawtooth period was fixed at 40 msec, and the self-consistently determined sawtooth mixing radii were 0.32, 0.37, 0.44, and 0.51 m for the currents listed above. It is clear that for  $q(a) \geq 3$  the sawtooth effects are modest, while for  $q(a) \leq 2$  they are very large. Evidently, the periodic current redistribution caused by the internal disruptions effectively "shorts out" some of the internal inductance of the plasma, and the relaxation time scale is reduced accordingly.

This qualitatively explains why the observed relaxation time scales in TFTR<sup>7</sup> are much less than given by Eq. (23a) for discharges with  $q(a) \leq 2.5$ .

## VII. SUMMARY

The time scales for current relaxation in toroidal plasmas have been calculated for three types of tokamak operation. These types are, in order of descending time scale, free decay of the plasma current, constant surface voltage, constant plasma current. These time scales are well represented over a wide range of plasma conductivity profiles by simple approximations (see Sec. V.D).

The principle limitations of this study are the neglect of (1) the effects of "sawtooth" internal disruptions, (2) time-varying plasma conductivity, and (3) toroidal and noncircular geometrical corrections to the cylindrical current diffusion equation. Experimental evidence and the calculations described in Sec. VI suggest that when the sawtooth mixing region extends to half the plasma minor radius or more, the relaxation time scale is greatly reduced; but if  $q(a) \geq 3$ , sawteeth have little effect.

## ACKNOWLEDGMENTS

It is a pleasure to thank M. Bell for useful discussions. This work is supported by the U.S. Department of Energy Contract No. DE-AC02-76-CHO-3073.

## REFERENCES

- <sup>1</sup>J.A. Schmidt, et al., "The Tokamak Fusion Core Experiment Studies," in Proceedings of the 10th Conference on Plasma Physics and Controlled Nuclear Fusion (IAEA, Vienna, 1985), Vol. 3, p. 297.
- <sup>2</sup>G. Bateman, MHD Instabilities, (MIT Press, Cambridge, MA, 1978).
- <sup>3</sup>H.P. Furth, P.H. Rutherford, and H. Selberg, Phys. Fluids 16, 1054 (1973) .
- <sup>4</sup>B.B. Kadomtsev, Sov. J. Plasma Phys. 1, 389 (1975).
- <sup>5</sup>C.E. Singer, D.E. Post, D.R. Mikkelsen, M. Redi, A. McKinney, A. Silverman, F. Seidl, P.H. Rutherford, R.J. Hawryluk, W.D. Langer, L. Foote, D.B. Heifetz, W. Houlberg, M. Hughes, R. Jensen, G. Lister, and J. Ogden, "BALDUR: One-Dimensional Plasma Transport Code," Princeton Plasma Physics Laboratory Report No. PPPL-2073 (July 1986), (submitted to Comput. Phys. Comm.).
- <sup>6</sup>S.P. Hirshman, R.J. Hawryluk, and B. Birge, Nucl. Fusion 17, 611 (1977).
- <sup>7</sup>M. G. Bell, private communication (1985).

TABLE 1.

Free Current Decay Eigenvalues for  $\sigma(r) = \text{constant}$ 

$k_{\text{ext}}^*$	$A^{k_1^2}$	$A^{k_2^2}$	$A^{k_3^2}$
0.5	3.641	21.18	56.55
1.0	1.577	16.64	51.21
2.0	0.885	15.67	50.22

## FIGURE CAPTIONS

- FIG. 1. The three families of conductivity profile shapes for  $q^* = 1.5, 2, 3, 4,$  and  $6$ : (a)  $\tilde{\sigma}_I$ , (b)  $\tilde{\sigma}_{II}$ , (c)  $\tilde{\sigma}_{III}$ . The "internal inductance,"  $\ell_i^*/2$ , is shown in (d) as a function of  $q^*$  for each conductivity family.
- FIG. 2. Free current decay eigenfunctions for  $\tilde{\sigma}_I$ ,  $q^* = 1.5, 2, 3, 4, 6,$  and  $\ell_{ext}^* = 1$ : (a)  $A_1(x)$ , (b)  $A_2(x)$ , (c)  $A_3(x)$ , (d)  $A_1(x)$  for  $\ell_{ext}^* = 0.5$ . As  $q^*$  rises, the eigenfunctions are progressively steeper for  $x \sim 0$ .
- FIG. 3. Constant surface voltage eigenfunctions for  $\tilde{\sigma}_I$ , and  $q^* = 1.5, 2, 3, 4, 6$ : (a)  $B_1(x)$ , (b)  $B_2(x)$ , (c)  $B_3(x)$ . As  $q^*$  rises, the eigenfunctions are progressively steeper for  $x \sim 0$ .
- FIG. 4. Constant plasma current eigenfunctions for  $\tilde{\sigma}_I$ , and  $q^* = 1.5, 2, 3, 4, 6$ : (a)  $C_1(x)$ , (b)  $C_2(x)$ , (c)  $C_3(x)$ . As  $q^*$  rises, the eigenfunctions are progressively steeper for  $x \sim 0$ .
- FIG. 5. Correction factor  $R_n$  [Eq. (24)] for  $\ell_{ext}^* = 0.5$ : (a)  $A\tilde{\tau}_1$ , (b)  $A\tilde{\tau}_2$ , (c)  $A\tilde{\tau}_3$ ; and for  $\ell_{ext}^* = 1$ : (d)  $A\tilde{\tau}_1$ , (e)  $A\tilde{\tau}_2$ , (f)  $A\tilde{\tau}_3$ . Curve label denotes the conductivity family.
- FIG. 6. Correction factor  $R_n$  [Eq. (24)]: (a)  $B\tilde{\tau}_1$ , (b)  $B\tilde{\tau}_2$ , (c)  $B\tilde{\tau}_3$ , (d)  $C\tilde{\tau}_1$ , (e)  $C\tilde{\tau}_2$ , (f)  $C\tilde{\tau}_3$ . Curve label denotes the conductivity family.
- FIG. 7. The simulated surface voltage during current "flat-top" after "ramp-up" for: (a)  $q(a) = 2.5$ , and (b)  $q(a) = 2.25$  (see Sec. VI for details).

#86P0260

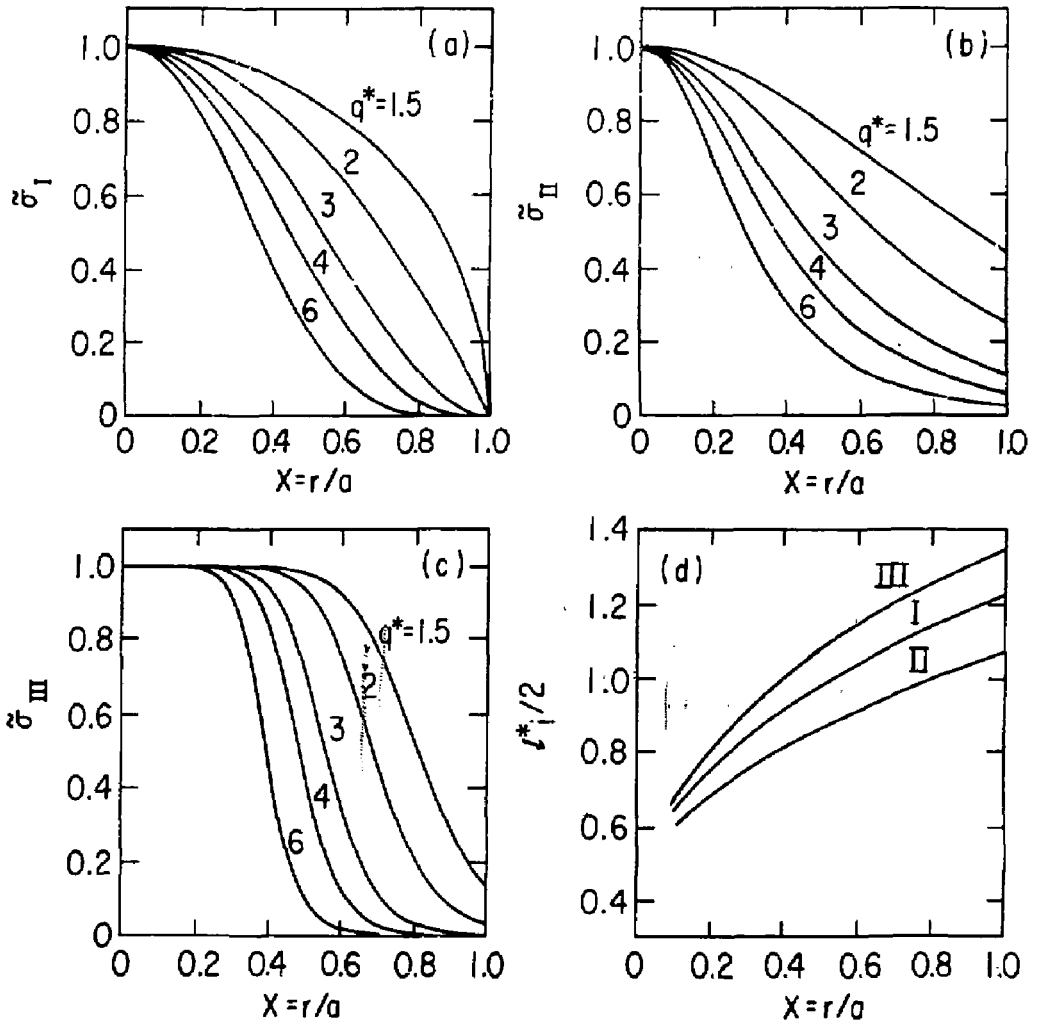


FIG. 1

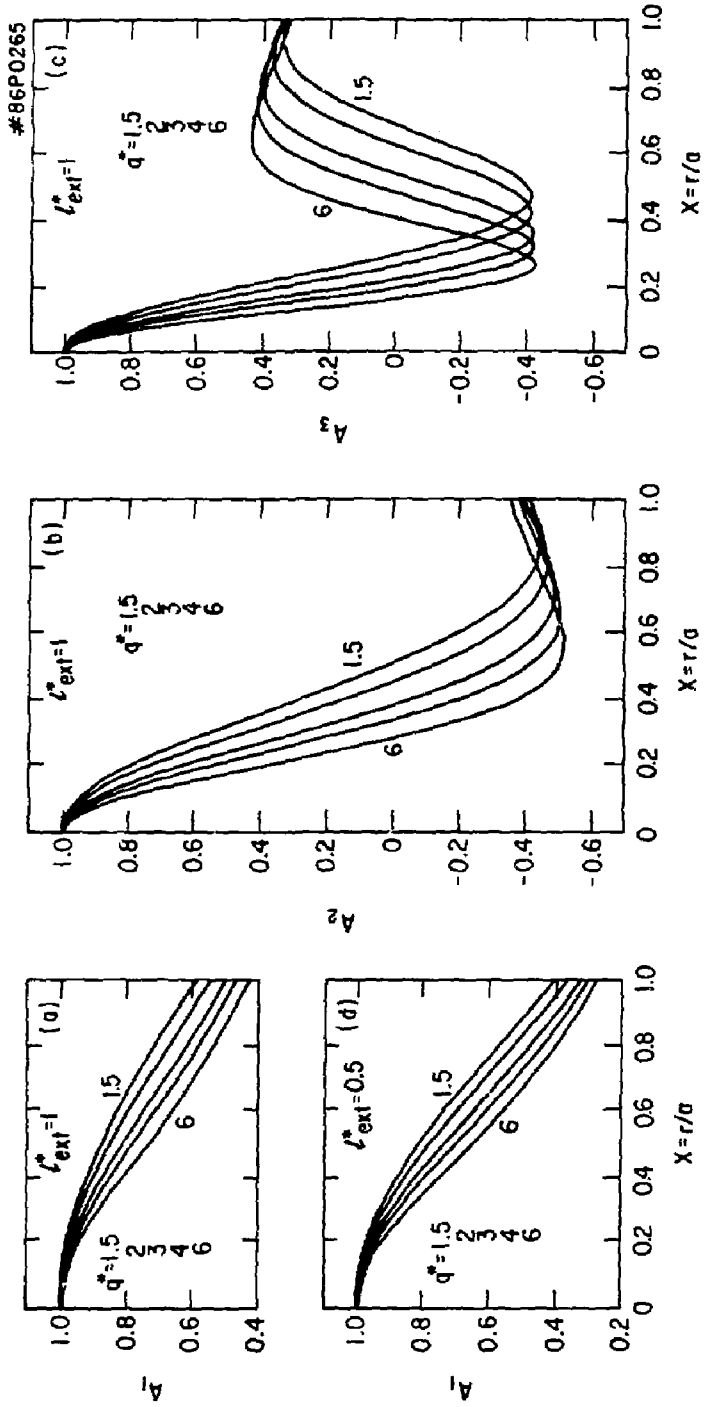


FIG. 2

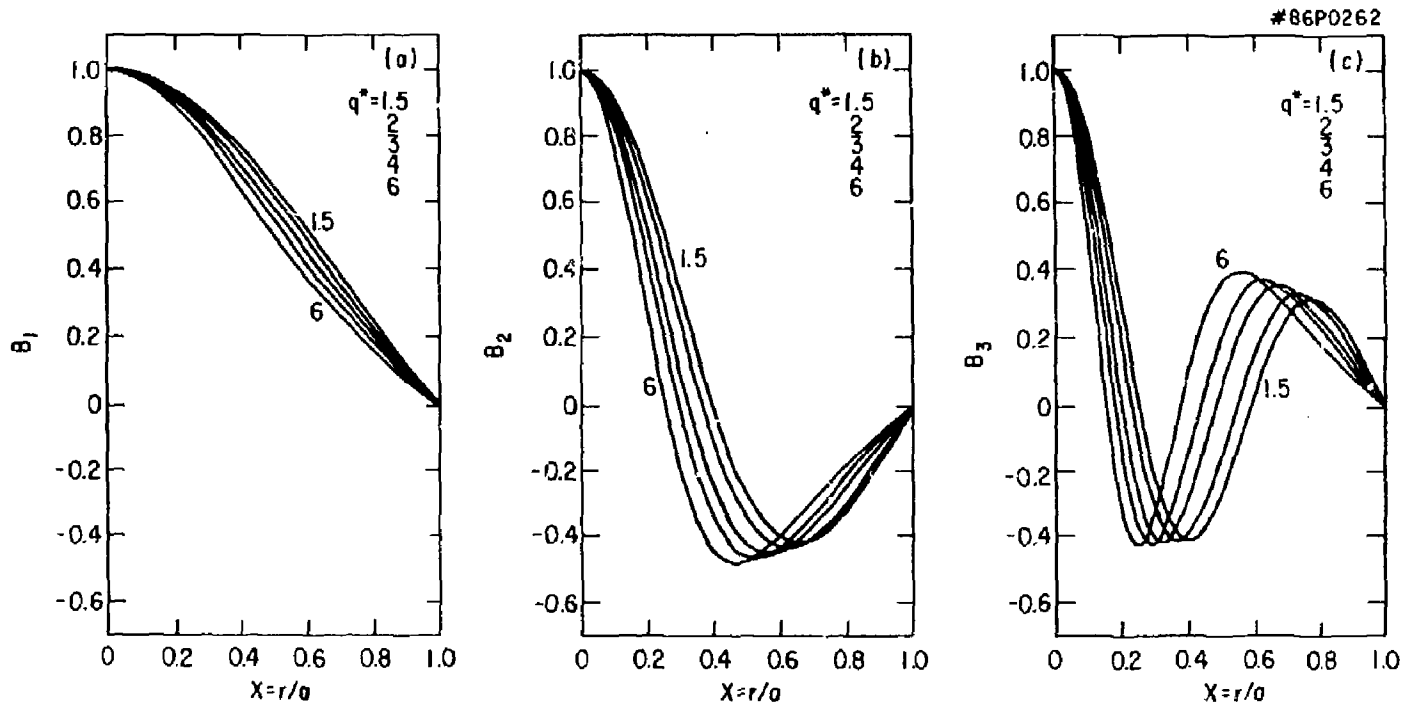


FIG. 3



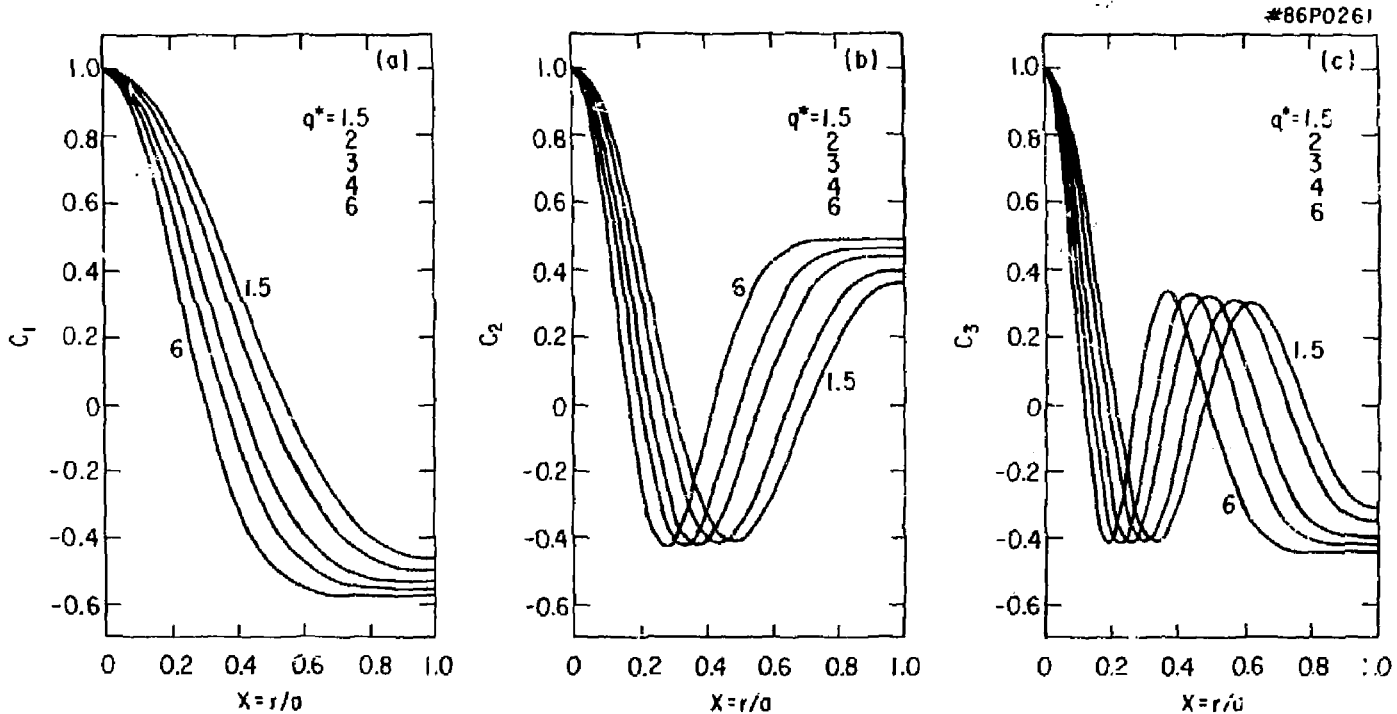


FIG. 4

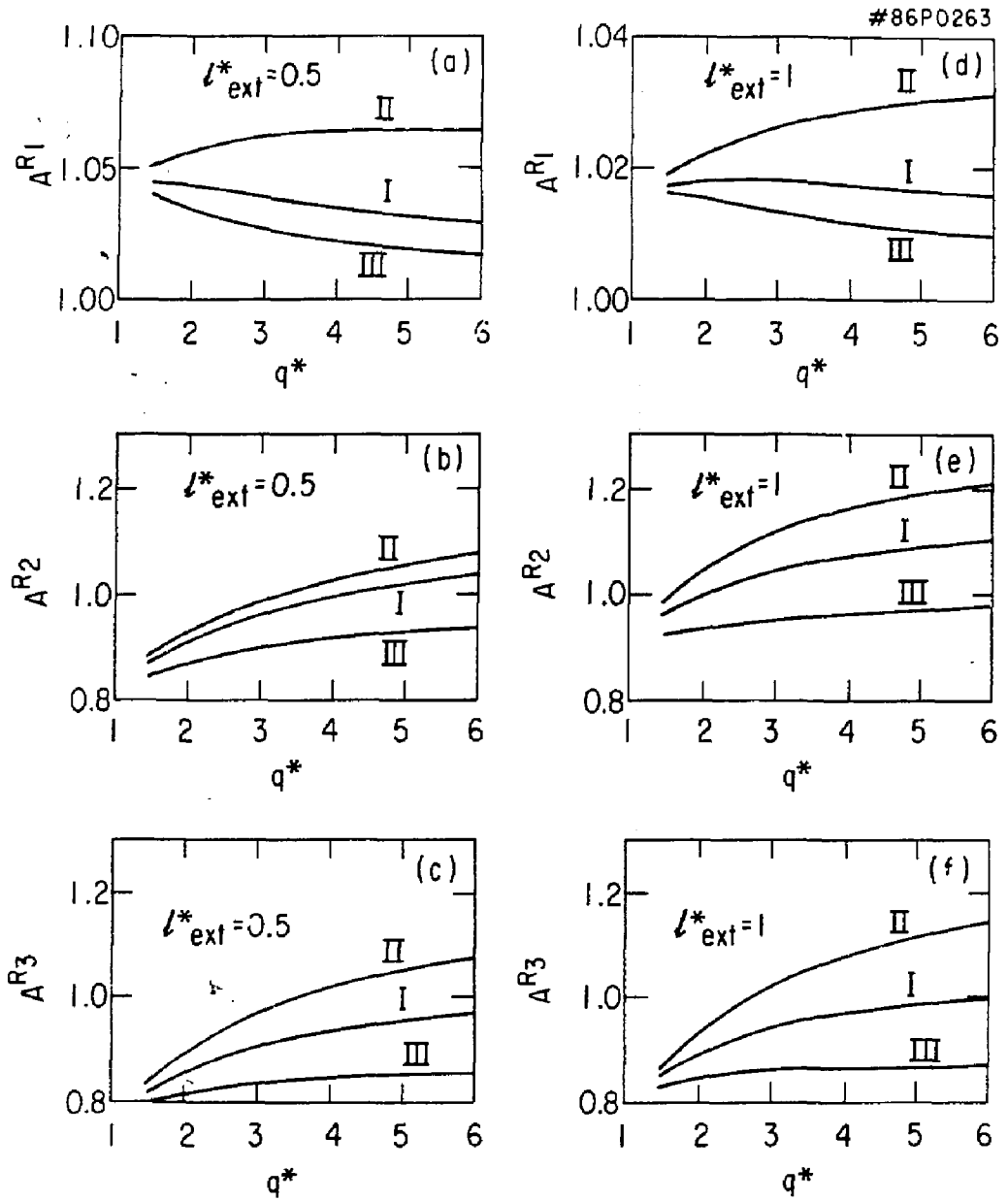


FIG. 5

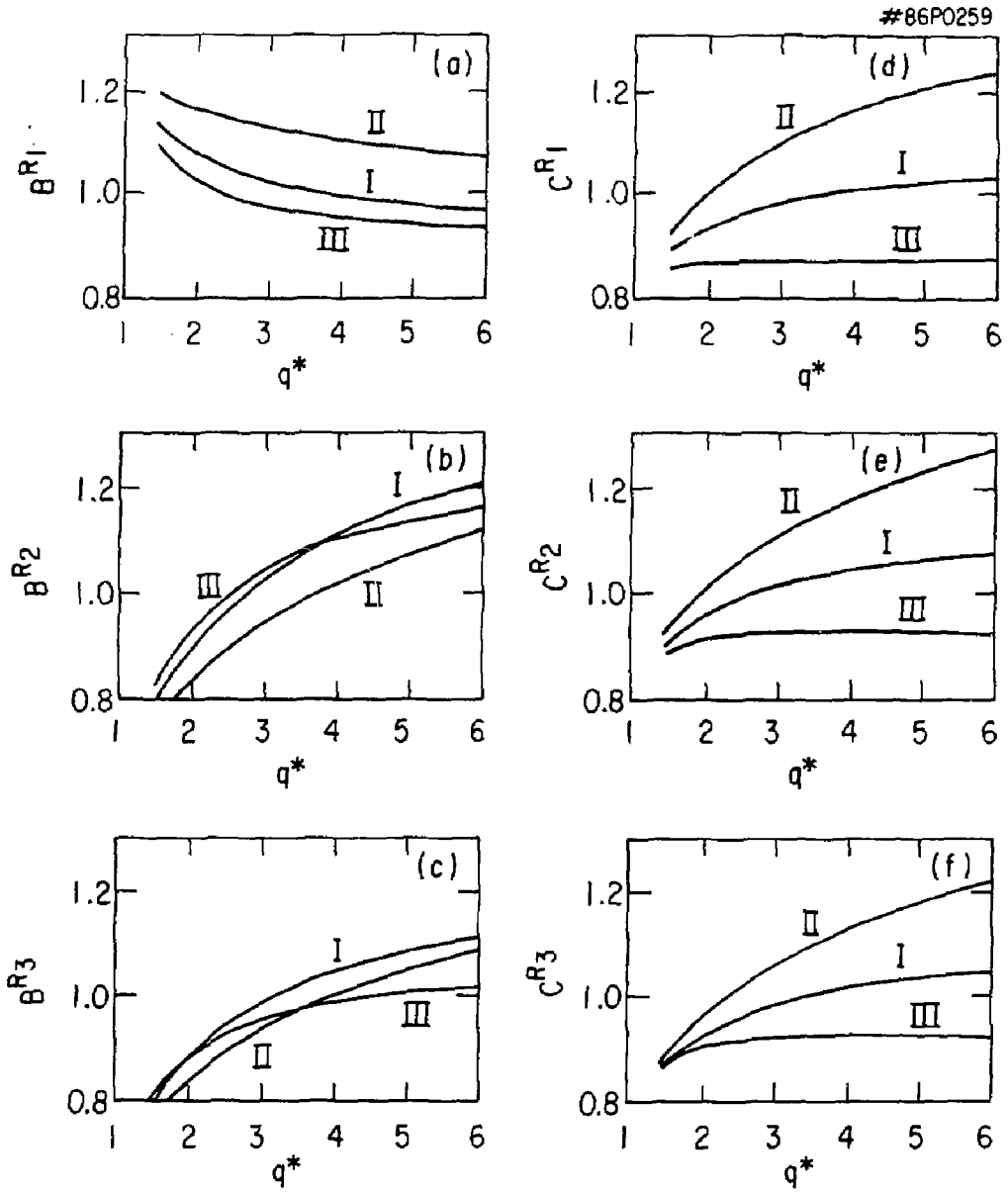


FIG. 6

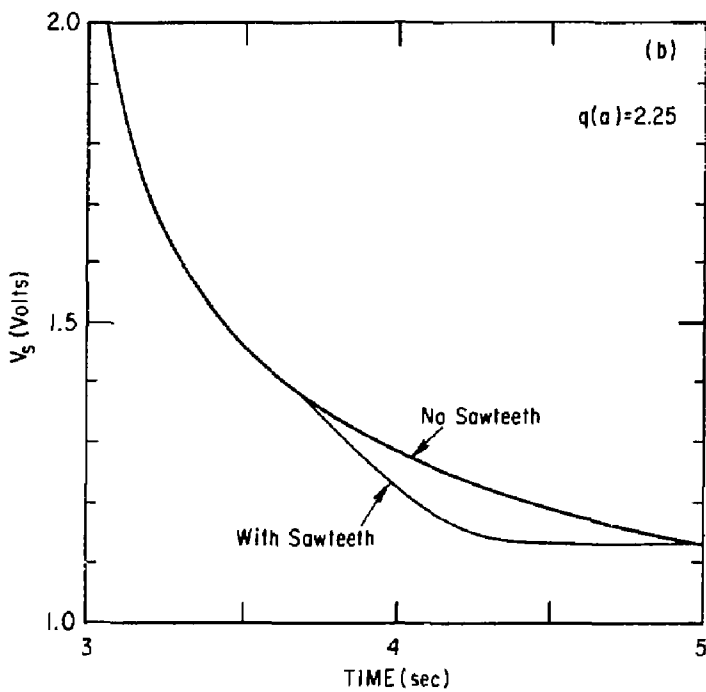
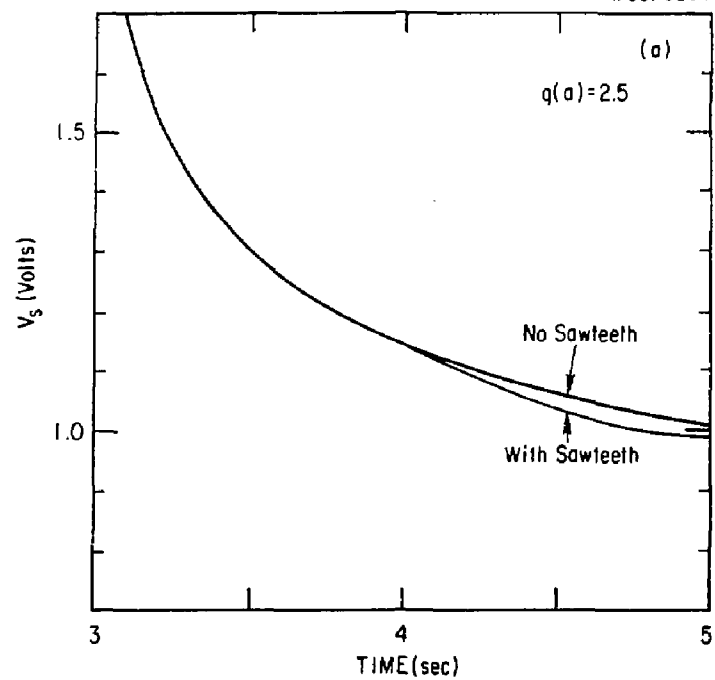


FIG. 7

EXTERNAL DISTRIBUTION IN ADDITION TO UC-20

Dr. Frank J. Paoloni, Univ of Wollongong, AUSTRALIA  
Prof. M.H. Brennan, Univ Sydney, AUSTRALIA  
Plasma Research Lab., Australian Nat. Univ., AUSTRALIA  
Prof. I.R. Jones, Flinders Univ., AUSTRALIA  
Prof. F. Čad, Inst Theo Phys, AUSTRIA  
Prof. M. Heindler, Institut für Theoretische Physik, AUSTRIA  
M. Goossens, Astronomisch Instituut, BELGIUM  
Ecole Royale Militaire, Lab de Phys Plasmas, BELGIUM  
Com. of European, Dg XII Fusion Prog, BELGIUM  
Prof. R. Bouclique, Laboratorium voor Natuurkunde, BELGIUM  
Dr. P.H. Sakanaka, Univ Estadual, BRAZIL  
Instituto De Pesquisas Espaciais-INPE, BRAZIL  
Library, Atomic Energy of Canada Limited, CANADA  
Dr. M.P. Bachynski, MPB Technologies, Inc., CANADA  
Dr. H.M. Skarsgard, Univ of Saskatchewan, CANADA  
Dr. H. Barnard, University of British Columbia, CANADA  
Prof. J. Teichmann, Univ. of Montreal, CANADA  
Prof. S.R. Sreenivasan, University of Calgary, CANADA  
Prof. Tudor W. Johnston, INRS-Energie, CANADA  
Dr. C.R. James, Univ. of Alberta, CANADA  
Dr. Peter Lukac, Komenského Univ, CZECHOSLOVAKIA  
The Librarian, Culham Laboratory, ENGLAND  
Mrs. S.A. Hutchinson, JET Library, ENGLAND  
C. Mouttet, Lab. de Physique des Milieux Ionises, FRANCE  
J. Radet, CEN/CADARACHE - Bat 506, FRANCE  
Dr. Tom Mual, Academy Bibliographic, HONG KONG  
Preprint Library, Cent Res Inst Phys, HUNGARY  
Dr. B. Dasgupta, Saha Inst, INDIA  
Dr. R.K. Chhajlani, Vikram Univ, INDIA  
Dr. P. Kaw, Institute for Plasma Research, INDIA  
Dr. Phillip Rosenau, Israel Inst Tech, ISRAEL  
Prof. S. Cuperman, Tel Aviv University, ISRAEL  
Librarian, Int'l Ctr Theo Phys, ITALY  
Prof. G. Rostagni, Univ DI Padova, ITALY  
Miss Clelia De Palo, Assoc EURATOM-ENEA, ITALY  
Biblioteca, del CNR EURATOM, ITALY  
Dr. H. Yamato, Toshiba Res & Dev, JAPAN  
Prof. I. Kawakami, Atomic Energy Res. Institute, JAPAN  
Prof. Kyoji Nishikawa, Univ of Hiroshima, JAPAN  
Direc. Dept. Lg. Tokamak Res. JAERI, JAPAN  
Prof. Satoshi Itoh, Kyushu University, JAPAN  
Research Info Center, Nagoya University, JAPAN  
Prof. S. Tanaka, Kyoto University, JAPAN  
Library, Kyoto University, JAPAN  
Prof. Nobuyuki Inoue, University of Tokyo, JAPAN  
S. Mori, JAERI, JAPAN  
M.H. Kim, Korea Advanced Energy Research Institute, KOREA  
Prof. D.I. Chol, Adv. Inst Sci & Tech, KOREA  
Prof. B.S. Liley, University of Waikato, NEW ZEALAND  
Institute of Plasma Physics, PEOPLE'S REPUBLIC OF CHINA  
Librarian, Institute of Phys., PEOPLE'S REPUBLIC OF CHINA  
Library, Tsing Hua University, PEOPLE'S REPUBLIC OF CHINA  
Z. Li, Southwest Inst. Physics, PEOPLE'S REPUBLIC OF CHINA  
Prof. J.A.C. Cabral, Inst Superior Tecn, PORTUGAL  
Dr. Octavian Petrus, AL I CUZA University, ROMANIA  
Dr. Johan de Villiers, Plasma Physics, AEC, SO AFRICA  
Prof. M.A. Hellberg, University of Natal, SO AFRICA  
Fusion Div. Library, JEN, SPAIN  
Dr. Lennart Stenflo, University of UMEA, SWEDEN  
Library, Royal Inst Tech, SWEDEN  
Prof. Hans Wilhelmson, Chalmers Univ Tech, SWEDEN  
Centre Phys des Plasmas, Ecole Polytech Fed, SWITZERLAND  
Bibliotheek, Fon-inst Voor Plasma-Fysica, THE NETHERLANDS  
Dr. O.O. Rytov, Siberian Acad Sci, USSR  
Dr. G.A. Eliseev, Kurchatov Institute, USSR  
Dr. V.A. Glukhikh, Inst Electro-Physical, USSR  
Dr. V.T. Tolok, Inst. Phys. Tech. USSR  
Dr. L.M. Kovrizhnykh, Institute Gen. Physics, USSR  
Prof. T.J.M. Boyd, Univ College N Wales, WALES  
Nuclear Res. Establishment, Jülich Ltd., W. GERMANY  
Bibliothek, Inst. für Plasmaforschung, W. GERMANY  
Dr. K. Schindler, Ruhr Universitat, W. GERMANY  
ASDEX Reading Rm, IPP/Max-Planck-Institut für  
Plasmaphysik, W. GERMANY  
Librarian, Max-Planck Institut, W. GERMANY  
Prof. R.K. Janav, Inst Phys, YUGOSLAVIA